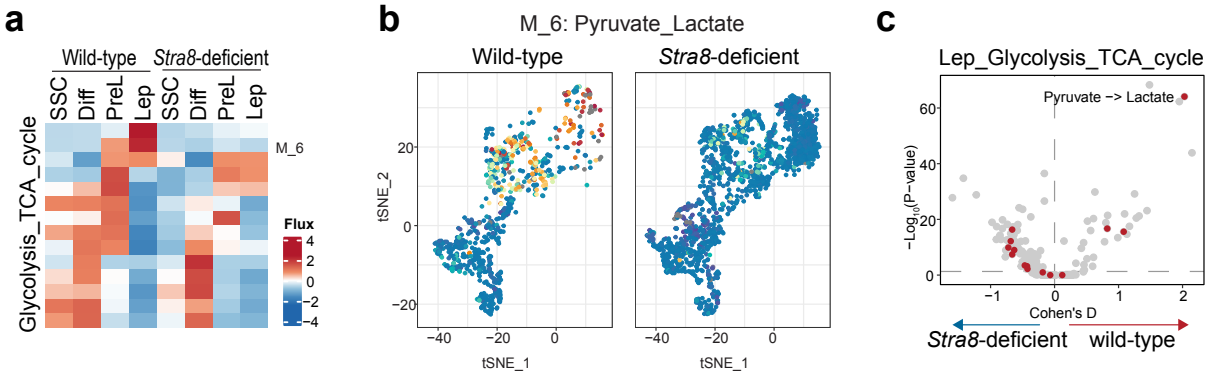

Supplementary Figure 1

Supplementary Figure 1. *Stra8* deficiency alters metabolic reprogramming in testicular germ cells.

a, Heatmap of predicted metabolic fluxes for glycolysis, the TCA cycle, and Pyruvate–Lactate conversion (M_6) across testicular germ cell types (SSC, Diff, PreL, Lep) in wild-type and Stra8-deficient mice. Red and blue indicate high and low flux, respectively. **b**, tSNE projection of single cells colored by Pyruvate–Lactate conversion flux (M_6). Wild-type cells exhibit distinct populations with high metabolic flux, which are largely absent in *Stra8*-deficient cells. **c**, Volcano plot showing differentially activated metabolic reactions in Leptotene (Lep) spermatocytes between wild-type and Stra8-deficient testes. Significant reactions are highlighted in red; notably, the conversion of pyruvate to lactate is significantly activated in wild-type cells (positive Cohen's D).

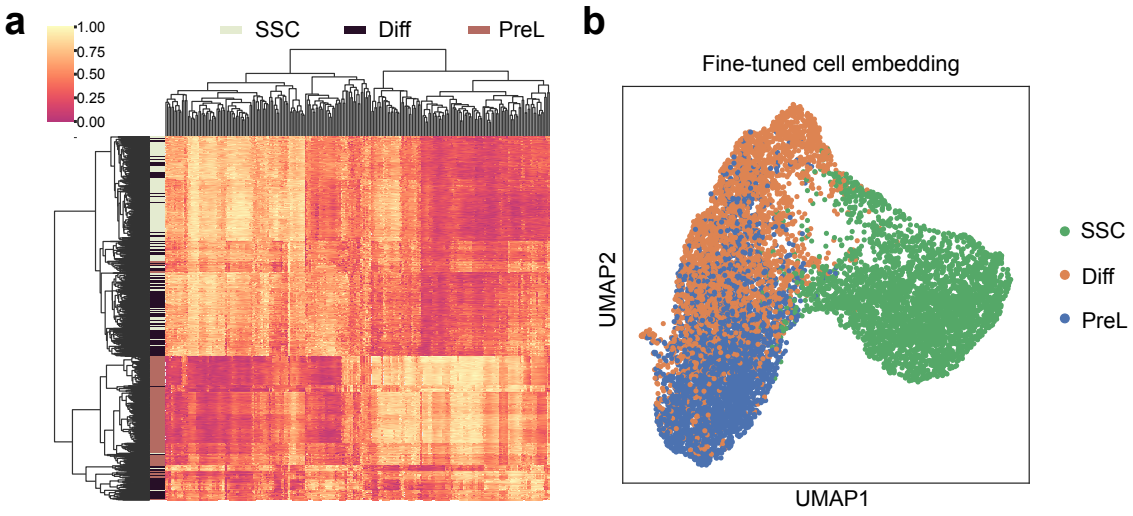

Supplementary Figure 2

Supplementary Figure 2. Transcriptomic profiling and fine-tuned embedding of early spermatogenic cell populations.

a, Hierarchical clustering heatmap of gene expression profiles across three distinct cell populations: spermatogonial stem cells (SSC), differentiating spermatogonia (Diff), and preleptotene spermatocytes (PreL). The color scale represents normalized expression levels, illustrating distinct transcriptomic signatures for each cell type. **b**, UMAP visualization of fine-tuned cell embeddings, demonstrating the clear transcriptomic separation and developmental trajectories of SSCs (green), Diff (orange), and PreL (blue) cells.

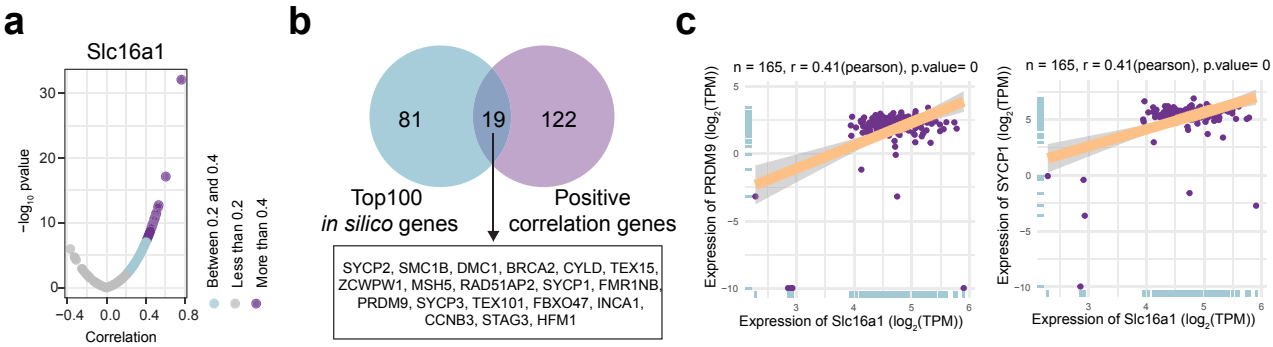

Supplementary Figure 3

Supplementary Figure 3. Identification of meiotic genes co-expressed with *Slc16a1*.

a, Volcano plot showing the correlation of genes co-expressed with *Slc16a1*. The x-axis represents the correlation coefficient, and the y-axis represents the significance level ($-\log_{10}$ *P*-value). Data points are color-coded by the strength of the correlation. **b**, Venn diagram illustrating the intersection between the top 100 in silico predicted genes and genes positively correlated with Slc16a1. The 19 overlapping genes, which are associated with meiotic processes, are listed below. **c**, Scatter plots demonstrating significant positive correlations between *Slc16a1expression* and two key meiotic markers, *PRDM9* and *SYCP1* (n = 165, r = 0.41, P = 0). Pearson correlation analysis was used.

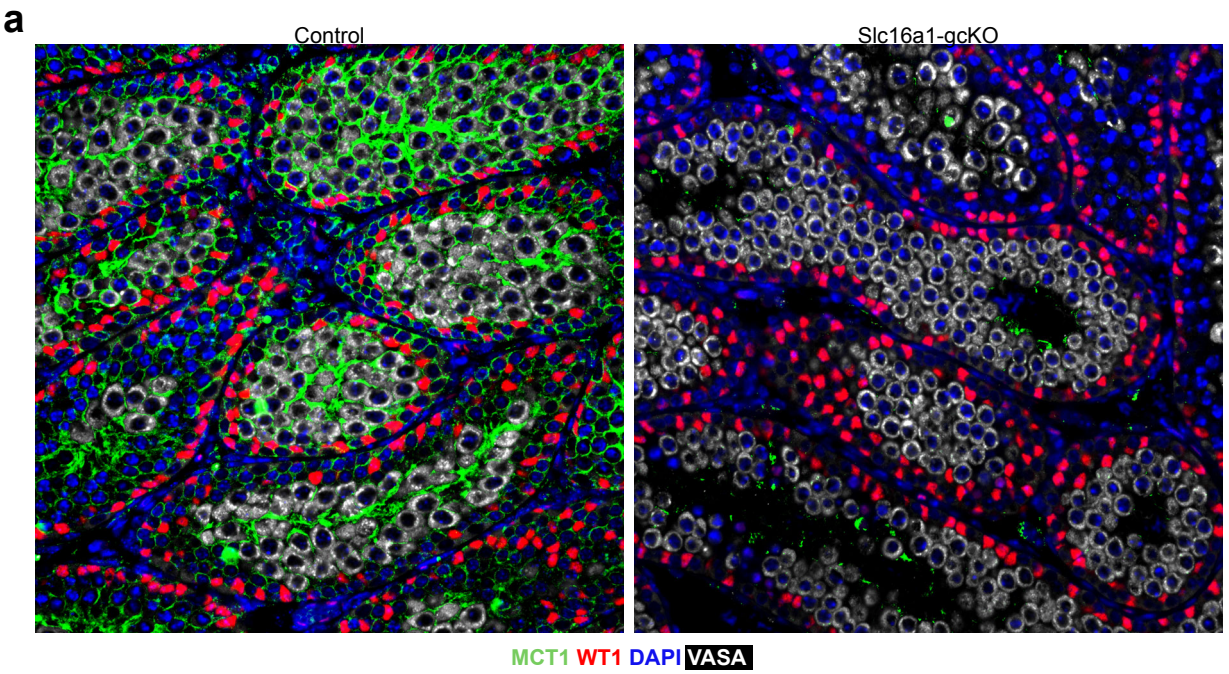

Supplementary Figure 4

Supplementary Figure 4: Germ cell-specific deletion of *Slc16a1* results in spermatogenic failure.

a, Representative immunofluorescence images of Slc16a1 (green) and WT1 (red) in control and Slc16a1-gcKO testis sections. DAPI (blue) marks nuclei. The absence of Slc16a1 signal in the Slc16a1-gcKO group confirms successful conditional knockout, while WT1-positive Sertoli cells are retained. **b**, Representative H&E-stained histological sections of seminiferous tubules from control and Slc16a1-gcKO mice. Slc16a1-gcKO testes exhibit severe seminiferous tubule atrophy, extensive germ cell depletion, and vacuolization compared to the organized, full spermatogenesis observed in controls. Scale bars, 50 μm.

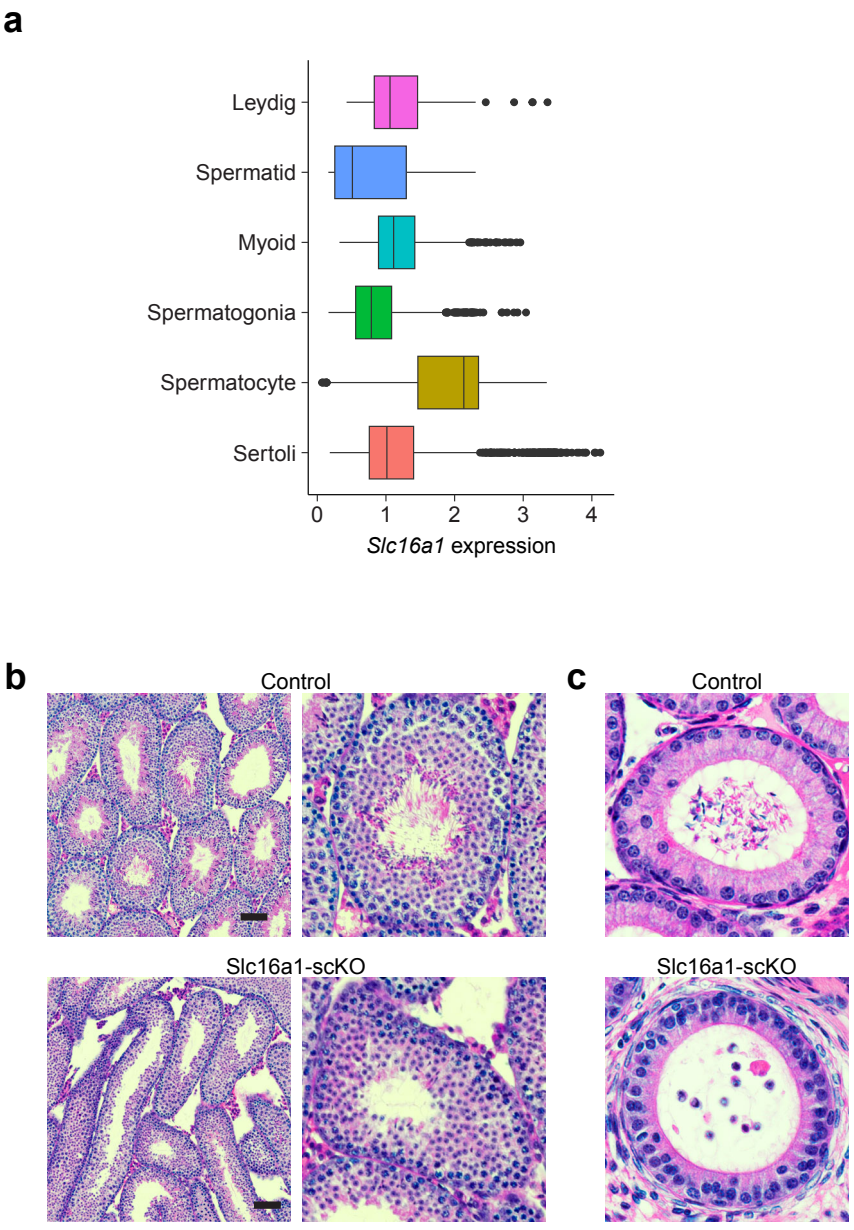

Supplementary Figure 5

Supplementary Figure 5. *Slc16a1* expression profile and the impact of somatic cell-specific deletion on spermatogenesis.

a, Box plot showing the single-cell expression levels of *Slc16a1* across distinct testicular cell populations, with spermatocytes exhibiting the highest expression levels. **b**, Representative H&E-stained cross-sections of seminiferous tubules from control and Slc16a1-scKO mice. Slc16a1-scKO testes display severe tubular atrophy and a marked depletion of germ cells compared to the robust spermatogenesis observed in control testes. Scale bars, 50 μm.

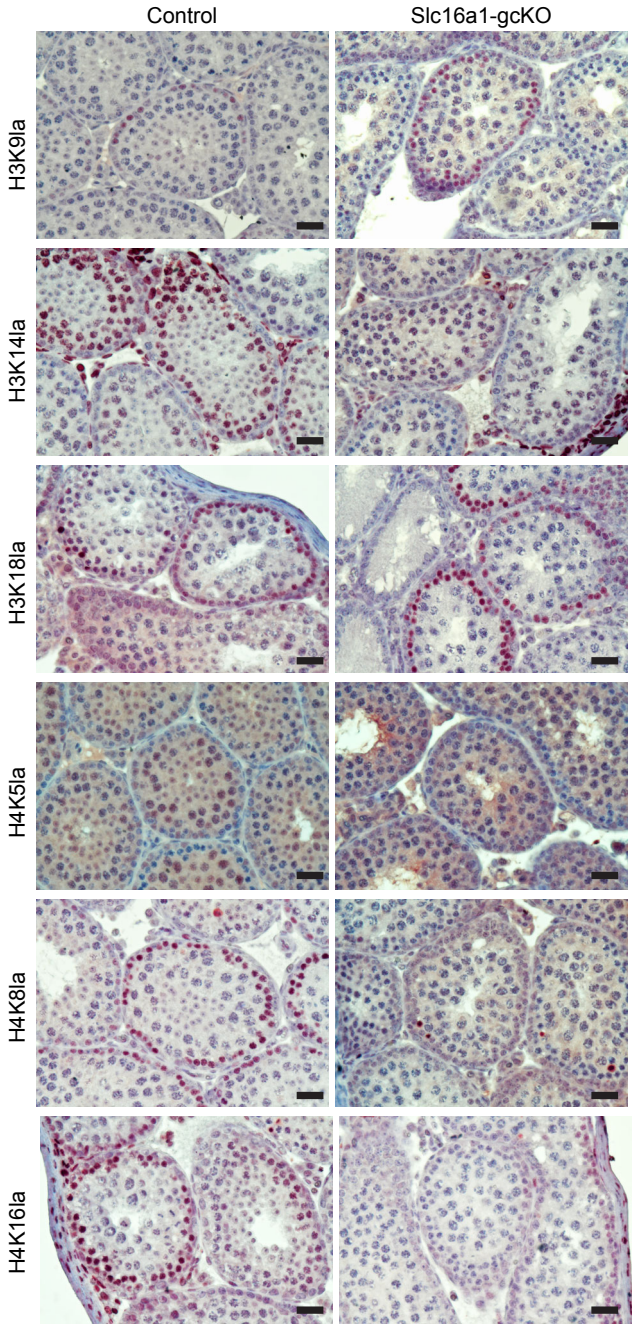

Supplementary Figure 6

Supplementary Figure 6. *Slc16a1* deficiency alters the histone lactylation landscape in the testis.

Representative immunohistochemical staining of various histone lactylation marks (H3K9la, H3K14la, H3K18la, H4K5la, H4K8la, and H4K16la) in testicular sections from Control and Slc16a1-gcKO mice. The germ cell-specific deletion of Slc16a1 leads to differential changes in the abundance and localization of these histone marks, indicating that Slc16a1-mediated lactate transport is essential for maintaining specific histone lactylation profiles during spermatogenesis. Scale bars, 50 μm.